Spray characteristics and penetration of the human cough, and the effectiveness of masks to prevent its dispersion

Raul Payri[a], Jaime Gimeno[a], Pedro Martí-Aldaraví[a,*], Javier Marco-Gimeno[a]

[a]*CMT-Motores Térmicos, Universitat Politècnica de València*

Abstract

Air-transmitted pathogens have become of particular interest for the general population during the COVID pandemic. Coughing is one of the most important spreading vector for air transmitted pathogens. To prevent and stop the transmission chain, it is of great importance to understand the characteristics of this phenomenon, assess the distance up to which the virion particles are transported and how effective the available masks are to stop the exhaled air. The Schlieren method stands as a proper non-intrusive methodology to study density variations such as the ones produced by the cough. An intubation dummy was instrumentalized to exhale CO_2 at realistic cough flow-rates and ambient conditions. General spray characteristics were obtained for a free cough, while effectiveness of a cloth, surgical and FFP2 masks were assessed by analysing the penetration and the angle of the exhaled fluid into the surrounding air. The differences between the propagation distances with and without mask were quantified. The characteristics of a free cough where firstly assessed, and later, the effectiveness of wearing a mask is shown, a cloth one reduces the cough penetration a 50%, while a surgical and FFP2 one reduces it more than an 75%, to less than 10 cm.

Keywords: Cough, Experimental, Schlieren, Spray, Masks, Effectiveness

1. Introduction

With the heightened interest in the transmission ways of air-distributed viruses such as the well-known influenza, or the new coronavirus SARS-CoV-2, it is useful to understand the characteristics of the human cough, and the available elements to prevent the dispersion of pathogens. These pathogens are located within the expelled saliva droplets during exhalations such as breathing, coughing or sneezing [1]. In air transmitted infections, coughs do emit up to 5000 virus-carrying droplets [2] and transport them within the cough itself [3]. These particles cover a wide range of sizes. Studies did not perfectly agree on a specific size distribution as it changed considerably from experiment to experiment [2, 4, 5, 6, 7, 8]. Nonetheless, there is an agreement on the predominance of small droplets (smaller than 20 µm). These particles are commonly known as aerosols, which are the main virus spreaders, as the larger particles are affected by gravity and quickly fall to the ground [9], while the dynamics of small particles are controlled by the characteristics of the expiratory event, and they easily remain airborne for long periods of time [10], which can increase the contagion risk in closed spaces. The turbulent structures created by the cough are responsible specially for these airborne particles and their dispersion across the closed room [11]. The presence of local air streams induced by local ventilation machines can modify the deposition times of these droplets, as the diffusion of the expelled droplets is remarkably enhanced after certain amount of time [12], and it mainly depends on the local turbulence intensity and length scales in this type of ventilated environments [13].

Several studies have focused their effort on obtaining information regarding mechanical, macroscopic and microscopic characteristics of the cough. Gupta et al. [14] performed an experimental campaign to characterize the cough flow rate of 25 male and female participants by means of spirometer. A mathematical expression could be extracted out of it, depending on the Peak Velocity Time (PVT), Cough Peak Flow Rate (CPFR) and the Cough Expired Volume (CEV), which is useful to determine boundary conditions in computational methods. Additionally, constant cough

*Corresponding author

direction between the subjects, as well as invariant mouth opening area were reported. Similar work was performed by Ren et al. [15], which after capturing the flow rate profile of 42 healthy participants, could approximate the curves by a piece-wise Gauss function which depended on the very same parameters as [14], CPFR, PVT and CEV with an accuracy over a 90%. Computational work has been performed by Wei et al. [16] to assess the droplet trajectories, and reported travelling distances higher than 2 m for small droplets, being purely transported by the cough air flow. Oliveira et al. [17] agrees on the dependency of settling times of aerosols on air currents, but not on gravity, as its effects started to appear after 20 min. It was also stated to be unsafe to maintain 2 m separation without using protective masks. Further computational studies were done on the topic by Muthusamy et al. [18] regarding the cough dynamics in closed room conditions at ventilated conditions, and the effect of cloth masks, concluding that employing such mask reduces the contamination range to two-thirds of the unobstructed cough, although that the aerosolized particles could reach longer distances and remain suspended longer periods of time. Li et al. [19] on the other hand, discovered that the presence of a human body at a distance of 1 m enhances the downstream droplet dispersion due to the modification in the cough aerodynamics.

Experimental studies have also been performed to assess propagation distances. Verma et al. [20] employed a mannequin head to expel the cough, and the air used for it was doped with fog droplets. A laser sheet was projected into the head symmetry plane and the cough was recreated by means of a manual pump. Reported travelled distances were as high as 3.65 m, although most of the droplets had already fallen to the ground by that point. Several commercial and hand made masks were tested, reducing notably the previous travel distances. Other non-intrusive studies have been also conducted. Wang et al. [9] performed two different types of experimental campaigns, by using image visualization, Particle Image Velocimetry and Particle Shadow Tracking Velocimetry (PIV and PSTV respectively). Interaction between the cough and the surrounding air was studied by means of air entrainment. The dependency of the cough distance from the emitter with time was found to be of $t^{0.3}$, which differed from the results obtained by Bourouriba et al. [21], which stated to be $t^{0.5}$ when the cough was dominated by jet-stream dynamics, and $t^{0.25}$ when the cough was puff-like. Exhaust velocity studies have also been performed by Geoghegan et al. [22] through high speed imaging of several individuals, where peak velocities resulted in a maximum of $64\,\mathrm{m\,s^{-1}}$, and a minimum of $1\,\mathrm{m\,s^{-1}}$, but high variabilities in the results were reported not only between different test subjects but on the very same individual (55-65% and 25-35% respectively). VanSciver et al. [23] also studied cough exhaust velocities, and in this case, the maximum reported velocity was of $29\,\mathrm{m\,s^{-1}}$, while the minimum was $1.5\,\mathrm{m\,s^{-1}}$. In this case, no angle was defined, but a spray thickness, whose average value ranged from 35 mm to 45 mm for the 29 participants. Dudalski et al. [24] obtained cough exhaust velocities using hot wire anemometry on several healthy and sick test subjects at a distance of 1 m from the mouth. A peak velocity of $1.2\,\mathrm{m\,s^{-1}}$ was found across all participants, in concordance with previous studies, and an average spread angle of 24°, which was similar to the values obtained by Gupta et al. [14]. No significant variations in the velocities and angles was found in sick, convalescent or healthy participants. Simha et al. [25] employed Schlieren imaging to detect the extent of cough propagation. 5 human test subjects were used for coughing. Several protection elements, such as hands covering mouths and protective masks were used. Lengths up to 3 meters were reported for unobstructed coughs. These kind of respirators need to meet the filtration standards, such as the particulate filtration, bacterial filtration and viral filtration [26]. Other studies [27] have further assessed the efficacy of such masks by setting up a single-pass Schlieren technique as well, indicating that all the masks reduce significantly the contaminated area, highlighting the importance of a proper fitting of the masks to minimize the cough spread.

The presented literature on experimental work shows studies performed mainly on human participants, which have shown to introduce high variability in the reported velocities and cough flow rate profiles. In order to obtain qualitative and quantitative parameters of the cough, a Schlieren imaging setup has been used to detect density gradients from the exhaust gases of a mannequin, replicating the human cough. To ensure realistic coughs, the gas flow rate has been measured to match Gupta et al. [14] cough profiles. The aim of the study is to extract macroscopic information of the cough, such as the penetration length into the ambient air, its angle, and to compare this information with the same information obtained after covering the mannequin with 3 protective masks with different certification and protection levels in order to assess their effectiveness.

The document will be divided into the following sections: this part, the introduction where the state of the art of topics related to experimental and computational recreation of coughs is described. It will be followed up by the methodology, where the experimental rig will be described, as well as the post-processing techniques employed to extract the data. The results section will be later provided, in which the main findings will be reported. The

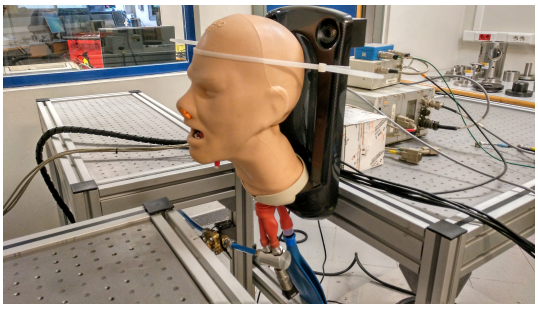

(a) Lateral view

(b) Frontal view

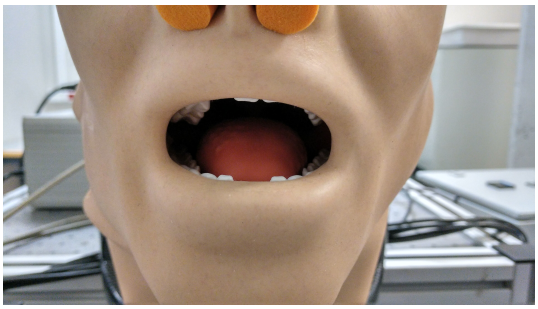

(c) Mouth close-up

Figure 1: Mannequin head employed for the replication of human coughs.

conclusions will conclude the document.

2. Methods

Schlieren imaging stands for a non-intrusive flow measuring technique that employs the change in direction that the light rays suffer when reaching a region with a different refractive index. This index is tightly related to the density through the Gladstone-Dale relationship [28]. By means of a spatial filter, which can be a razor edge or a diaphragm, these bended light rays are blocked out in the focal plane, while the undisturbed rays go through the filter. This principle permits to observe gaseous phases, which are not visible to the human eye, to become visible in the form of gray-scale colours. Therefore, this technique allows to accomplish the objectives of this work.

It would be useful to reduce the uncertainties derived from testing coughs from participants, while ensuring representative results. In order to ensure repeatability between the experiments and subtract the uncertainties that may arise from testing human participants, a mannequin head has been instrumentalized. The model employed for this purpose is Trucorp's AirSim Advance X. It is composed of a nose, a mouth and its internal elements (tongue and teeth) which could play an important role on inducing cough turbulence, and of modelled aerial cavities, consisting of the pharynx, larynx and trachea. The digestive system is also recreated down to the esophagus. Trachea is connected to a 3 L pressurized deposit which is connected to the gas tank. The frontal area of the mouth could be approximated to an ellipse with major and minor semi-axis of 2.5 cm and 1.5 cm respectively. The mouth has been oriented to expel the cough in an horizontal direction. The upper aerial ways have been blocked to stop the air to blow from the nose, as the aerosols expelled on coughing come mainly from the mouth [29]. Images of the described mannequin head have been included in Figure 1. The mannequin skin is set at ambient temperature, as the thermal plume should not have important effects on the cough jet during the first time instants, when the cough is momentum controlled.

To ensure that the refractive index of the expelled gaseous phase differs from the index of the remnant air, carbon dioxide (CO_2) has been used as the cough gas. The expelled CO_2 gas concentration during expiratory events is approximately of a 5% of the total volume [30]. The CO_2 should be a representative cough gas as long as the

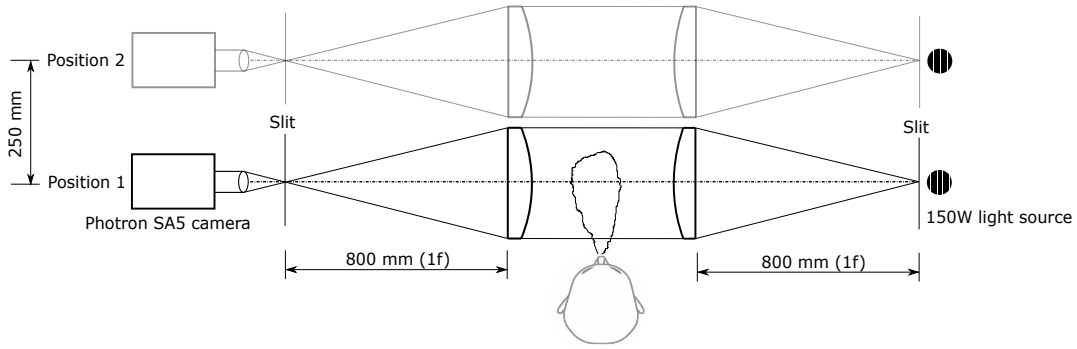

Figure 2: Scheme of the single pass Schlieren setup for the characterization of human coughs.

inertial forces control the event, until these forces are dissipated and the gravity starts to affect the exhaled gas. The cough temperature is dependent on the ambient temperature [31], nonetheless, the CO_2 is injected at room ambient temperature (25 °C) with an open-closed electro-valve, controlled with an Injection Control Unit (ICU). In addition to it, a KISTLER pressure sensor has been introduced prior to the trachea, capable of measuring up to 10 bar (gauge) to obtain the flow rate signal.

2.1. Schlieren optical setup

Two 200 mm of diameter, 800 mm of focal length and 0.13 numerical aperture convex lenses have been used to parallelize and focus the emitted light rays. It was arranged in a single pass configuration, which is shown in Figure 2. The two lenses have been placed at both sides of the mannequin head to set the region in which the light rays should be parallel. As the characteristic length of the human cough is larger than the lens diameter, the location of the lenses can be easily moved in the spray direction to obtain information at larger distances. The two positions used for the study are sketched in Figure 2. A 150 W DC-regulated halogen light source has been used to emit the light rays and a diaphragm has been placed after the light source to obtain a point source. The second diaphragm acts as the knife edge that will block deflected light beams. Being a radial spatial filter, it will cut out both vertical and horizontal density gradients.

A 1024x1024 pixel high speed camera has been located after the knife edge to capture the non-deflected beams. A 50 mm lens is attached to the camera to properly focus the image. The recordings have been captured at a frame rate of 1000 fps, which is enough to capture the spray flow dynamics, which ranges from 100 Hz to 900 Hz [32]. The shutter speed value was set (33 µs) to obtain enough luminosity for the post-processing routines.

2.2. Cough flow rate profile characterization

To recreate realistic coughs with the presented experimental facility, the proper boundary conditions need to be defined. The flow rate time profiles experimentally obtained by Gupta et al. [14] have been selected for this purpose. A mathematical expression was derived from the mentioned profiles. This expression has been included on Equations 1 and 2. The parameters that compose these Equations are described in Table 1. From them, three different cough flow rate profiles have been extracted with the maximum, minimum and mean values reported in Table 2, that correspond to the strongest cough reported by male participants, the weakest cough reported by female coughs, and the mean values between the described coughs, respectively. These three curves should be able to represent the whole range of human coughs, and they are represented in Figure 3.

$$\bar{M} = \frac{a_1 \tau^{b-1} \exp\left(\frac{-\tau}{c_1}\right)}{\Gamma(b_1)\, c_1^{b_1}} \quad \text{for} \quad \tau < 1.2 \tag{1}$$

$$\bar{M} = \frac{a_1 \tau^{b-1} \exp\left(\frac{-\tau}{c_1}\right)}{\Gamma(b_1)\, c_1^{(}b_1)} + \frac{a_2 \left(\tau - 1.2\right)^{(b_2-1)} \exp\left(\frac{-(\tau-1.2)}{c_2}\right)}{\Gamma(b_2)\, c_2^{b_2}} \quad \text{for} \quad \tau > 1.2 \tag{2}$$

Parameter	Definition
$\overline{M}$	$\frac{FlowRate}{CPFR}$
τ	$\frac{Time}{PVT}$
a_1	1.680
b_1	3.338
c_1	0.428
a_2	$\frac{CEV}{PVT \times CPFR} - a_1$
b_2	$\frac{-2.158 \times CEV}{PVT \times CPFR} + 10.457$
c_2	$\frac{1.8}{b_2 - 1}$

Table 1: Parameters of Equations 1 and 2.

	Male		Female	
	Min.	Max.	Min.	Max.
CPFR [L/s]	3	8.5	1.6	6
CEV [L]	0.4	1.6	0.25	1.25
PVT [ms]	57	96	57	110

Table 2: Reported limits of cough flow parameters [14].

The first step to reproduce these profiles is the characterization of the flow rate in the described facility.

To do so, the pressure signal in the exhaust line has been measured, and according to Equation 4 [33], the desired mass flow rate has been obtained. To check the accuracy of the previous method, it has been measured the mass variation of the deposit during a pressure jump from 3 bar to 2 bar (gauge) by means of the ideal gas equation (Equation 4) and compared with the results of the theoretical procedure. Similar results were obtained by the two methods described, showing low deviation in the values.

Due to the use of an open/closed electro-valve, it is impossible to perfectly match the flow rate profile shape of the introduced curves. Therefore, the aim is to match the maximum peak flow rate and the total expired volume as the maximum to show the most similar profile possible. By matching the peak flow rate the same cough strength is achieved, which is one of the parameters that characterize mask filtration efficiency as evidence suggests [34]. The different flow rate profiles were achieved by modifying the deposit pressure and the electro-valve opening time. Five repetitions of each test point were acquired for the flow rate characterization and image processing. Figure 3 shows the comparison between the selected profiles [14] and the experimentally obtained curves. The associated boundary conditions to the presented curves are shown in Table 3. The open/closed electro-valves do not allow to perfectly recreate the mathematical model curves, which induce step-like functions on the experimental curves, with a sudden increase up to close-to-CPFR values, and then a sudden drop after the valve has closed. Therefore it has been matched the total gas volume expired, as well as the peak flow rate. The comparison between the experimental flow rate obtain by the facility described and the mathematical expression of Gupta et al. study [14], are shown in Table 4. Moreover, an additional comparison of the CPFR values between the literature curves and the experimental ones has been included in Table 5. The CPFR are slightly higher for the experimental results both in the maximum and mean flow rates, although the differences are slightly higher than the 15% for both cases. With respect the minimum CPFR profile, the results are accurately matched, leading to an error of a 2.5%. An overall agreement both in the time profile shape and the total expired fluid volume was obtained, leading to realistic cough expiration through the experimental facility.

$$PV = nRT \tag{3}$$

$$\dot{m} = C_d \cdot A \sqrt{2\rho\Delta p} \tag{4}$$

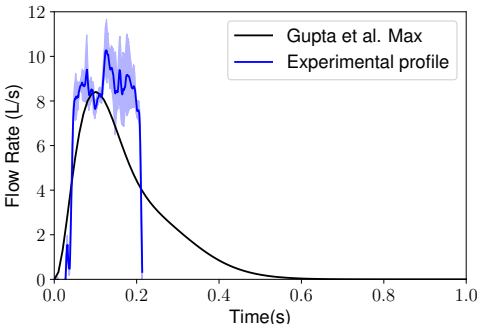

(a) Maximum Flow Rate Profile

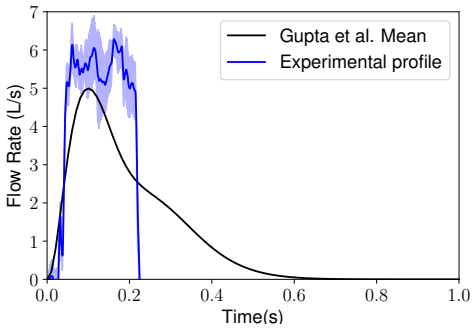

(b) Mean Flow Rate Profile

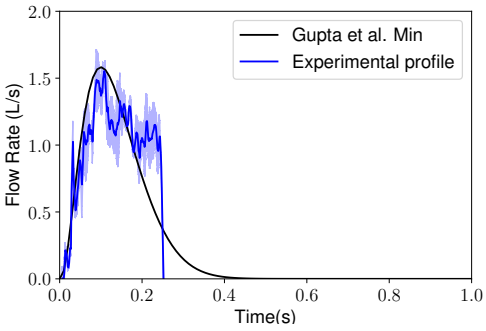

(c) Minimum Flow Rate Profile

Figure 3: Flow Rate comparison between the experimental and Gupta et al. [14] profiles.

	Injection Pressure (gauge)	Valve Opening Time
Maximum Peak Flow Rate profile	2.2 bar	0.14 s
Mean Peak Flow Rate profile	1.7 bar	0.15 s
Minimum Peak Flow Rate profile	1.0 bar	0.18 s

Table 3: Boundary conditions associated to the three experimentally obtained curves.

	Experimental	Gupta et al.
Maximum Peak Flow Rate profile (CPFR=8.5 L s^{-1})	1.45 L	1.66 L
Mean Peak Flow Rate profile (CPFR=5 L s^{-1})	0.989 L	1.09 L
Minimum Peak Flow Rate profile (CPFR=1.6 L s^{-1})	0.25 L	0.26 L

Table 4: Fluid expired volume comparison between the Gupta et al. [14] curves, and the values obtained in the test rig.

	Experimental	Gupta et al.
Maximum Peak Flow Rate profile	10.21 L s^{-1}	8.5 L s^{-1}
Mean Peak Flow Rate profile	6.19 L s^{-1}	5.05 L s^{-1}
Minimum Peak Flow Rate profile	1.56 L	1.6 L s^{-1}

Table 5: Cough Peak Flow Rate values comparison between the Gupta et al. [14] curves, and the values obtained in the test rig.

2.3. Image processing

The processing of the captured frames is a key process to properly analyse the information [35]. The method employed for the Schlieren analysis [36] segments the spray and the background. Once the segmentation has been finished, variables such as the penetration, and spray angle among others can be obtained. This processing routine performs four tasks: image masking, background subtraction, contour detection and contour analysis. Figure 4 shows an example of the described procedure around a specific captured frame.

2.3.1. Background subtraction

The first step differentiates between the cough and the background image. This step is not straightforward for the Schlieren procedure as the background image could vary through the whole cough event, as any light ray that crosses any density gradient could be captured by the camera. The segmentation is performed based on an image-temporal-derivative approach [37], which is combined with a dynamic-background composition subtraction [38] by means of a weighting factor. Nonetheless, no background ventilation was set during the experimental procedure and this effect should not be of importance.

2.3.2. Image masking

The following procedure consists of identifying the region where the spray should be expected. In this way, undesired elements that may be present in the image can be omitted in the later processing steps. These elements might be the black area projected by the mouth, regions outside the illuminated window, etc. In this particular case, the mask has been defined by a 90° area, whose vertex is located at the mouth exit. The mask matrix, whose size equals the frame pixel matrix, multiplies the pixel illumination value by one where the region of interest is present, and by zero in the pixel where no information should be present.

2.3.3. Contour detection

In order to detect the cough contour, the images are binarized using the dynamic range of the frame, multiplied by a specified factor. Although the background image could have some structures that could be identified as part of the cough due to an imperfect background subtraction, a set of filters are also applied that remove small pixels regions (Figure 4c) and a erosion process to remove background noise (Figure 4d). After that, a dilation process is performed to counter-act the effect of the erosion process in the dimensions of the contour [37]. After this two-step ero-dilation process, the boundaries are identified as the spray contour, that is later applied to the original image, as seen in Figure 4f.

2.3.4. Data analysis

Once the contours have been extracted, macroscopic descriptors of the cough can be obtained from them. The cough penetration S is the leading position of the spray contour in the mouth normal direction of the images, indicated by the S parameter on Figure 5. On the other hand, the spread angle θ was calculated as the angle that composes a trapezium between two defined bases Figure 5. This bases are located at a 12% and a 50% of the spray penetration. Once the cough spray mixes with the ambient air, the density gradients become less evident, resulting in penetration and angle values that no longer characterize the flow of study.

2.4. Protective masks

Apart from the unobstructed cough event, three different commercially available masks have been attached to the mannequin head. First of all, a cloth mask (Figure 6a) that satisfies the European Norm CWA17553:2020 is used. Secondly, a standard surgical mask of IIR type (Figure 6b)[39] that protects against droplets and fluid splashes has also been tested. This masks are intended to protect patients from the possible pathogens exhaled by the medical team during a surgery. They do not fit tightly to the face of the user and are not intended to be used more than 8 hours [40]. At last, a Filtering Face Piece 2 (FFP2) respirator mask (Figure 6c) has been used. These masks are on the other hand intended to protect the user from the inhalation of pathogens, and are fitted to the face to prevent air leakage. According to European Standards (EN 149 [41]), FFP2 masks should be able to filter at least the 95% of the particles with a diameter larger than 0.3 μm. Although no droplets are going to be expelled through the experimental facility, efficiency of mask effectiveness can be assessed by analysing how far can the cough jet travel, as the local turbulence

Payri, R., Gimeno, J., Martí-Aldaraví, P., & Marco-Gimeno, J. (2021). Spray characteristics and penetration of the human cough, and the effectiveness of masks to prevent its dispersion. Building and Environment, 108584. https://doi.org/10.1016/j.buildenv.2021.108584

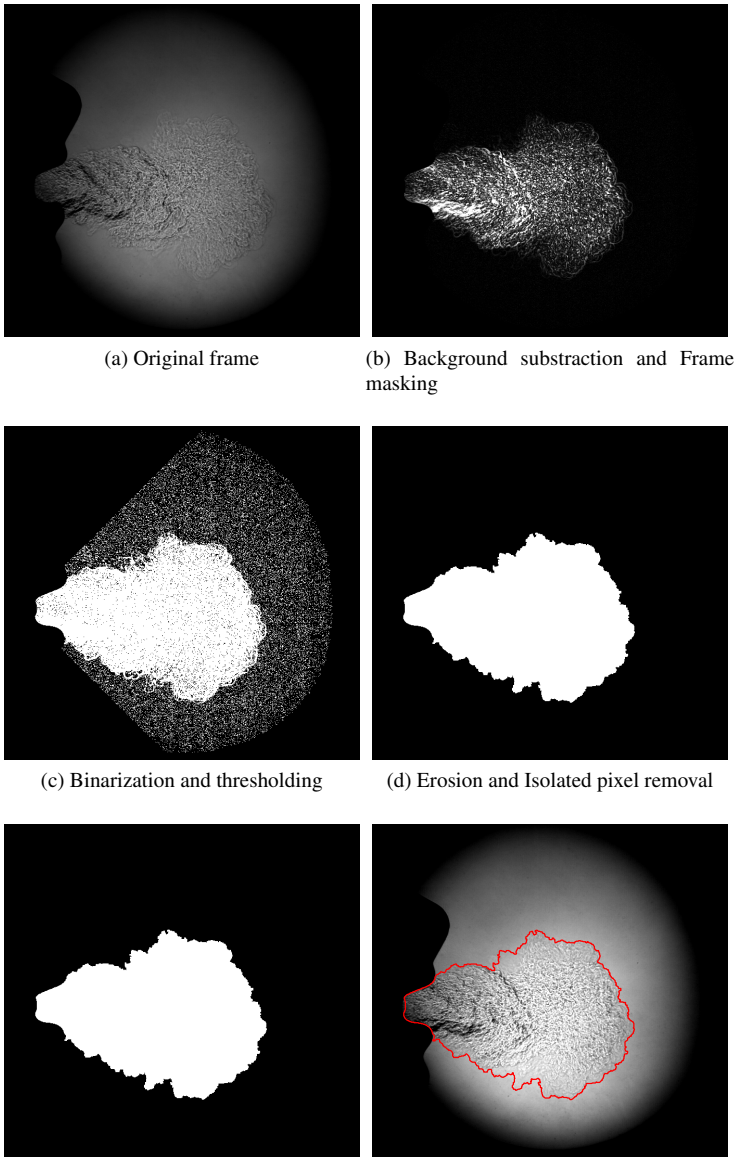

(a) Original frame

(b) Background substraction and Frame masking

(c) Binarization and thresholding

(d) Erosion and Isolated pixel removal

(e) Two-step dilation

(f) Contour result on original image

Figure 4: Contour detection algorithm process. The frame corresponds to a time of 0.06 s after the valve opening instant.

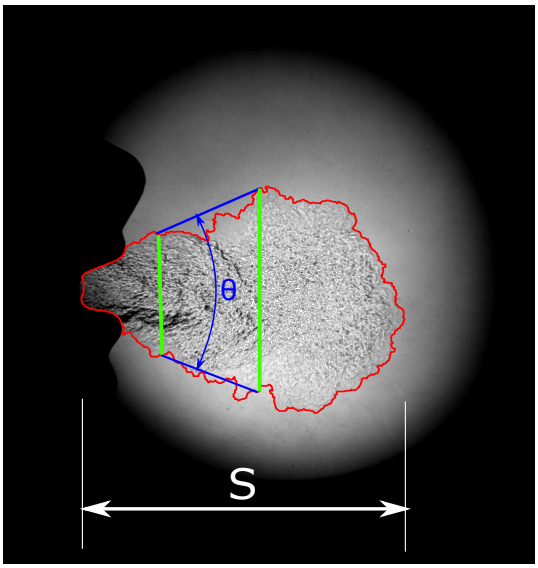

Figure 5: Scheme of the single pass Schlieren setup for the characterization of human coughs.

	Materials	Filtration Capabilities
Cloth Mask	3 Cloth Layer	70% particles larger than 3 µm
Surgical Mask	Non-woven fabric	98% particles larger than 3 µm
FFP2 respirator	Polypropylene	95% particles larger than 0.3 µm

Table 6: Material and filtration characteristics of the masks employed.

affects the dispersion of the airborne particles and are affected by the velocity field [11, 13]. In addition to it, local airflow is one of the responsible for virion suspension in air and transport [42]. Therefore, measuring the velocity and diffusion of air in the first time instants would give an insight on where the exhaled droplets would be if they happened to go through the masks. A summary of the filtration characteristics and materials of the masks employed is located at Table 6 regarding the face mask materials and filtrating capabilities.

3. Results and discussion

The three cough intensities have been captured with the Schlieren imaging technique for the free-cough case and with the described masks. The computed results consist of cough penetration for all the coughs and spray angle for the free-cough. Due to the limitation of obtaining cough data within the dimensions of the lenses employed, the visualization rig has firstly been set in the immediate zone of the mannequin head, and later it has been displaced 200 mm further in the cough exhaust direction. As the two viewing sections do not overlap, some gaps after 200 mm will be shown for the penetration plots, as it can be seen on Figure 2.

As the masks occupies a certain area from the visualization region, the penetration curves show the distance of the spray tip to the mask location, instead of respect to the mouth exit. The furthest axial position of these masks is included in Figure 7.

Payri, R., Gimeno, J., Martí-Aldaraví, P., & Marco-Gimeno, J. (2021). Spray characteristics and penetration of the human cough, and the effectiveness of masks to prevent its dispersion. Building and Environment, 108584. https://doi.org/10.1016/j.buildenv.2021.108584

(a) Cloth Mask

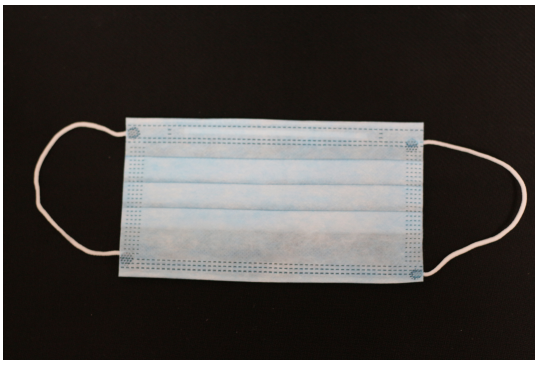

(b) IIR Surgical Mask

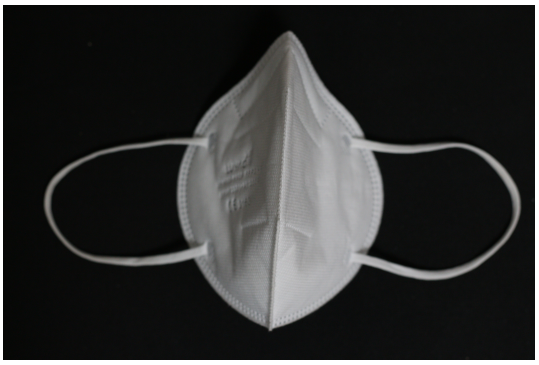

(c) FFP2 Respirator

Figure 6: Protective equipment tested during the experimental campaign.

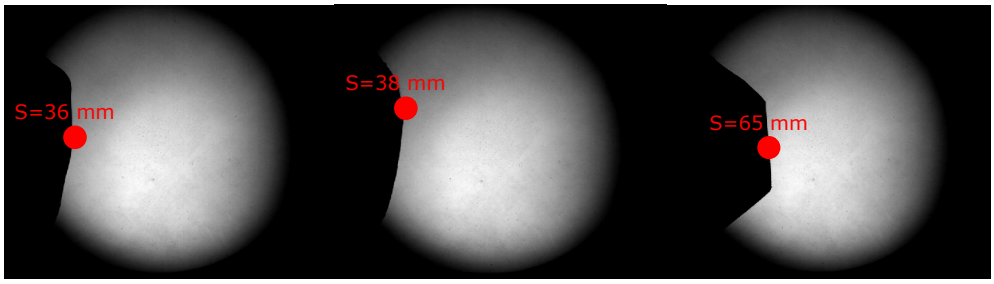

(a) Cloth mask (b) Surgical mask (c) FFP2 respirator

Figure 7: Location at which the penetration can be firstly detected for all the masks tested.

3.1. Unobstructed cough

Snapshots of the spray generated by the free cough have been taken to visually analyse the evolution of the exhaled fluid into the atmosphere. The visualization results for the cough associated to the maximum CPFR value have been included for both windows, and are shown in Figure 8. The case with a higher flow rate reaches the end of the first visualization window after 40 ms (Figure 8c), and the end of the second visualization window after 80 ms (Figure 8h). All three coughs show the same morphology, and not clear distinct spray angles, which indicates that the exhalation flow rate does not affect the cough widening. The contours detected in the second window follow the same trend, although some information is being lost below the measuring area. The minimum CPFR profile shows no cough activity in the second window until 100 ms after the cough start while the strongest cough has almost reached a penetration value of 400 mm at the specified time. Therefore, the distance at which the saliva droplets can travel, which are dispersed by the exhaled air, is highly dependent on the strength of the cough.

Figure 9a shows the evolution of the spray tip position along the two lenses. The three cough CPFR profiles have been included. The spray angle at the closest visualization region to the head has also been included in Figure 9b. The shaded area of both plots represents the standard deviation of the five repetitions performed. There is a clear difference between the three profiles tested. The maximum CPFR profile shows the steepest penetration evolution, as it reaches both 200 mm and 400 mm at approximate 45 ms and 150 ms. The mean CPFR profile shows lower velocities, reaching 400 mm at approximately 200 ms. On the other hand, the lowest CPFR time profile shows a more gradual slope, reaching the maximum measurable distance of the second visualization region at 350 ms. When it comes to the spray angle, two distinct phases are found. The first one prior to the 25 ms after the cough detection, where all three profiles show a peak in the angle value close to 60° for the maximum CPFR profile, and 45° for the minimum CPFR one. This probably corresponds to the toroidal recirculation region that is formed at the tip of the cough spray [20]. After that, all three curves stabilise around the same value, and no clear differences are found between them. An average angle of 32° is found, which is a larger value than the value obtained by Gupta et al. [14] and Dudalski et al. [24]. These differences arise due to the lower gas density of the surrounding air, compared to the higher density of the expelled CO_2 [43]. Nonetheless, the standard deviation contour shows high variability, with maximum values of 50° and minimum angles of 20°. Due to the high spray angle obtained for the first visualization window, part of the cough area lays outside of the second visualization window, which could lead to smaller cough angles than the real ones. Therefore, the angle values for the second window have not been calculated.

According to Bourouiba et al. [21], until 0.5 s the spray penetration shows a dependency with time of $S \propto t^{\frac{1}{2}}$. Regression curves have been obtained for each one of the three CPFR time profile tested. Figure 10 shows the three curves, which show the dependency with time to the power of 0.5, and they yield a R^2 coefficient higher than 0.99 in all cases, which coincides with the conclusions obtained by the previous study. The corresponding mathematical expressions have been included in the figure itself. On the other hand, from the penetration curves spray tip velocities have been obtained. Peak velocities fall within the reported ranges of Vansciver et al. [23] and Geoghegan et al. [22] as the minimum CPFR profile shows velocities higher than $1\,\mathrm{m\,s^{-1}}$. Wang et al. [9] reported maximum cough flow rate velocities of $10\,\mathrm{m\,s^{-1}}$. Chao et al. [4] reported on their experiments as well a maximum velocity of $13\,\mathrm{m\,s^{-1}}$. On the other hand, Dudalski et al. [24] reported a mean cough peak velocity of $1.2\,\mathrm{m\,s^{-1}}$ at a distance of 1 m from the mouth, which therefore shows great velocity drops at close distance to the mouth. Computational studies agree

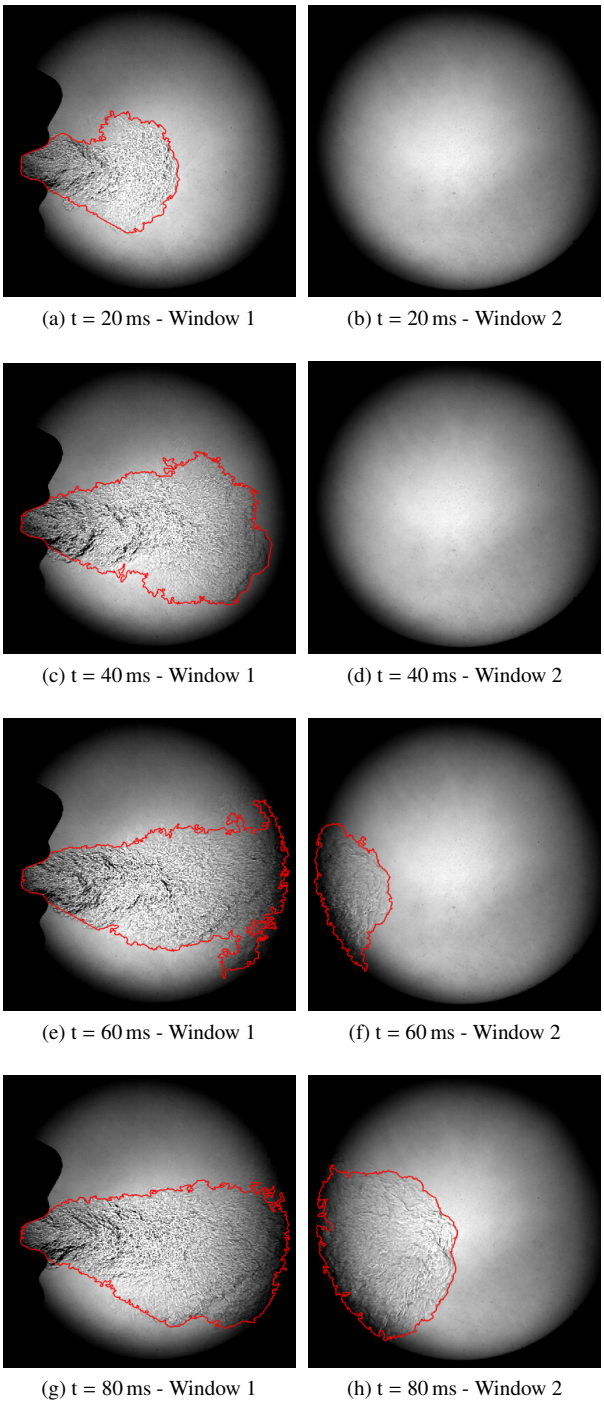

(a) t = 20 ms - Window 1 (b) t = 20 ms - Window 2

(c) t = 40 ms - Window 1 (d) t = 40 ms - Window 2

(e) t = 60 ms - Window 1 (f) t = 60 ms - Window 2

(g) t = 80 ms - Window 1 (h) t = 80 ms - Window 2

Figure 8: Time snapshots of the cough contour for the strongest cough flow rate profile at the two positions of the Schlieren experiment.

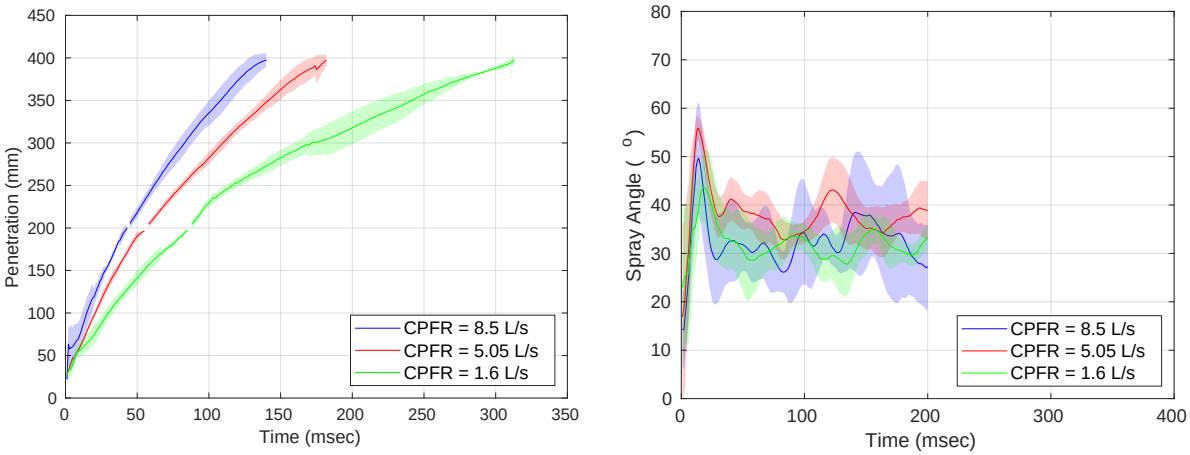

(a) Cough Penetration

(b) Cough angle

Figure 9: Evolution with time of the cough penetration and angle at three different injection flow rates for the free jet case.

on the strong velocity drop after the cough has been introduced into the surrounding air [44]. This, in addition to the high uncertainty in the penetration plot during the first cough instants derived from the low density gradients detected, explains the lower velocities obtained. The reason for having slightly lower peak flow velocities can rely on the strong drag effects on the cough, as it has been reported by Chillon et al. [45]. In addition to it, similar velocities cough tip velocities were reported by Tang et al. [46] for a typical male after 100 ms after cough exhalation, of approximately 3 m s^{-1}.

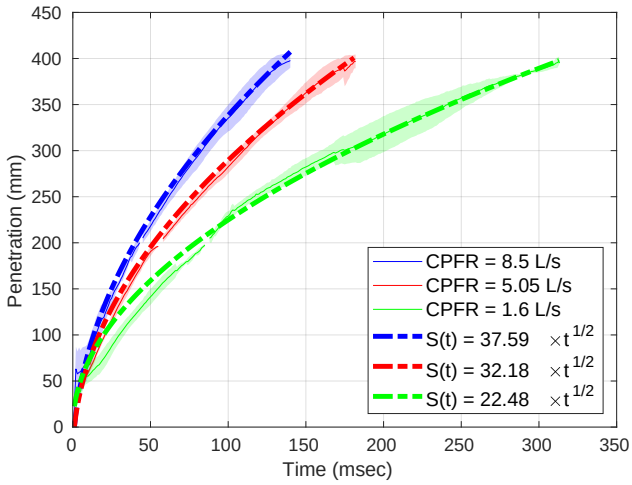

Figure 10: Penetration fitting curves for the free-cough case, at the three CPFR time profiles.

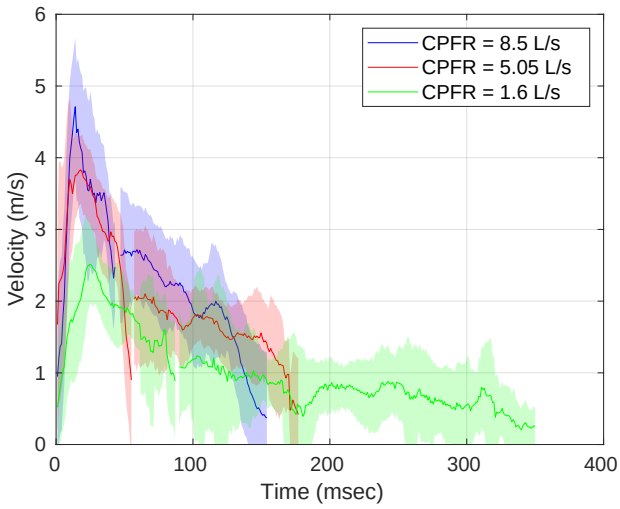

Figure 11: Velocity profile for the three CPFR time profiles.

3.2. Cloth mask

Four temporal snapshots are taken for each of the three cough profiles tested. Figure 12 depicts how the exhaled fluid is slowed down by the cloth equipment, its reach seems to be decimated, as after 160 ms its penetration has almost reached the end of the visualization region, but no more. Weaker cough profiles seem to follow the same trend, being significantly slowed down. The morphology of the cough has changed with respect to the free cough results, as the cone shape has disappeared. The exhaled air is introduced into the atmosphere through a large area of the mask, and not only through the section were the mouth is located. Figure 13 shows the distances travelled by the cough with respect to the mask that correspond to the contour snapshots described. All three curves show the expected reduction in the cough velocities, as the maximum CPFR profile takes 350 ms to cross the visualization window, compared to the 40 ms in the corresponding free cough case. The same happens with the other two cough intensities. In the weakest CPFR time profile, the density gradient has mostly dissipated after 400 ms which prevents the post-processing routine to detect the spray tip without high uncertainties. Contour detection on the second visualization distance (200 mm-400 mm) is not possible due to the same issue just mentioned, although some density gradients are slightly visible. Therefore it can be stated that the spray has travelled a total distance of 164 mm from the mask. The cloth mask employed therefore allows to slow down the cough velocities in all three cases, and reduce the penetration distance to half of the detected penetration in the free cough. A curve fitting has been also performed on the cloth penetration data, and its results have been included in Figure 13b. The dependency of the penetration on the expression $S(t) \propto t^{\frac{1}{2}}$ is not as strong as the dependencies shown for the unobstructed cough. The constants associated with the curve fitting are also reduced, as shown in the fitting expression.

3.3. Surgical mask

The corresponding time snapshots have also been included in Figure 14. Clear differences are observed with respect to the previous mask. The exhalation area is also increased with respect to the free cough case, but the velocity and total penetration distance is greatly reduced in the three cough intensities, although there are still mild penetration differences between the maximum CPFR and the minimum CPFR profile. After 160 ms, the cough has almost not penetrated into the visualization window, not even reaching half of the illuminated region even for the strongest cough, which indicates how the inertial forces have been dissipated by the surgical mask. The exhaled air ceases its movement in the vicinity of the mask, not reaching any further into the domain.

The distance to the mask curves included in Figure 15a are also analysed. The maximum CPFR profile does indeed reach further into the domain compared to the mean and weak coughs. In this case, the distance travelled by the cough spray from the mask outlet is of 30 mm, 25 mm and 12 mm for the maximum, mean and minimum flow profiles respectively. After a certain time, it can be stated that the cough has stopped penetrating, as the curves show

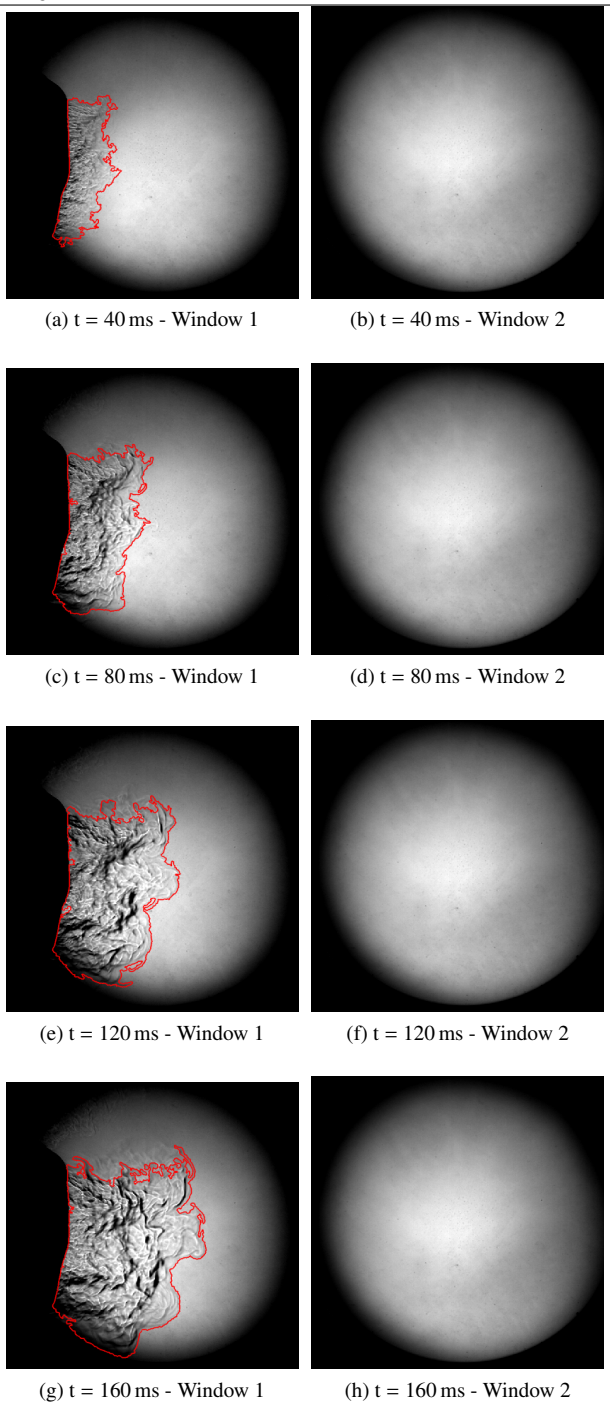

(a) t = 40 ms - Window 1 (b) t = 40 ms - Window 2

(c) t = 80 ms - Window 1 (d) t = 80 ms - Window 2

(e) t = 120 ms - Window 1 (f) t = 120 ms - Window 2

(g) t = 160 ms - Window 1 (h) t = 160 ms - Window 2

Figure 12: Time snapshots of the cough contour for the strongest flow rate profile time profile and the cloth mask at the two positions of the Schlieren experiment.

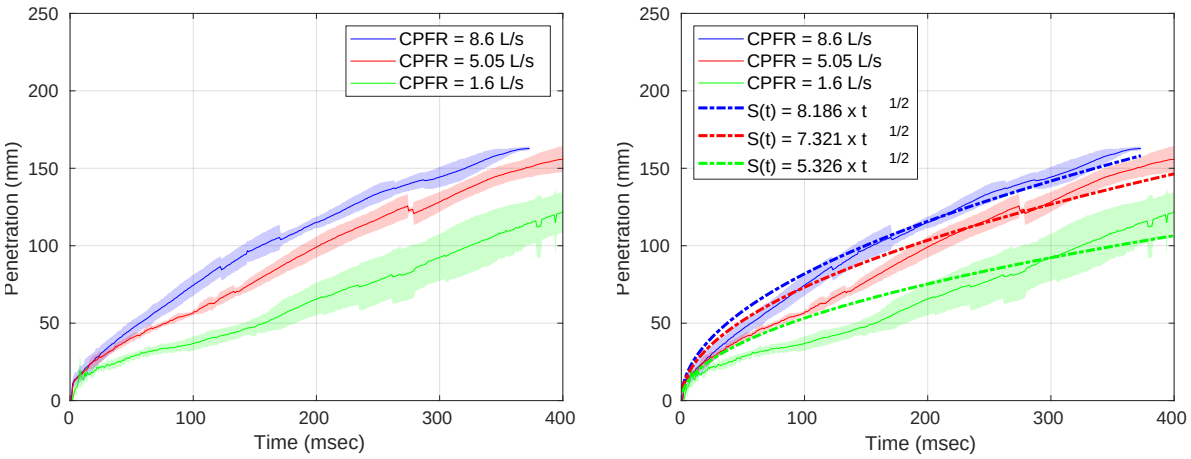

(a) Distance curves

(b) Curve fitting

Figure 13: Distances with respect to the cloth mask, at the three CPFR time profiles and its corresponding curve regression.

a time where the cough furthest reach starts to decrease. This happens for the CPFR = 8.5 L s^{-1} profile at 250 ms after the cough has been detected into the domain, 200 ms for the CPFR = 5.05 L s^{-1} profile, and 150 ms for the CPFR=1.6 L s^{-1} profile.

3.4. FFP2 respirator

Similar results were obtained for the FFP2 respirator employed. Figure 16 shows the corresponding time snapshots of the exhaled cough. It can be analysed how most of the exhaled gas is visualized in the regions were the mask fitting is not perfect, implying that some of the exhaled gas leaks through the nose and neck region and little cough is exhausted through the frontal region. For that reason, as those leakages are not representative to assess the cough reach, only the frontal area of the mask has been processed with this equipment. Nonetheless, for the maximum and mean CPFR profiles the cough is detected, and a similar distance is observed for both cases. After 80 ms the penetration seems to remain constant (Figure 16c), which indicates that the cough velocity almost negligible after this point. On the other hand, the minimum velocity profile has shown no contour at all. After a visual inspection, the density gradients induced by the exhaled cough are seen at the lower part of the respirator, but no shadows are observed through the frontal and upper region of the respirator. Therefore, in the distance to the mask plot (Figure 17a), only the curves that correspond to the maximum (CPFR = 8.6 L s^{-1}) and mean (CPFR = 5.05 L s^{-1}) time profiles have been included. The FFP2 respirator occupies a larger region of the illuminated area, and therefore the minimum penetration detected is 65 mm. The change in trend observed in the curve of the strongest cough at around 200 mm may be due to the interaction of the flow that is leaking through the nose clip and through the neck, and not because of the flow that goes through the respirator. Same happens with the mean CPFR profile, which starts to decrease its penetration after 150 mm, and a few milliseconds later it starts to rise again. The detected profiles have travelled a total of 21 mm and 18 mm for the maximum and mean CPFR profiles respectively.

Figure 18 shows all the penetration curves obtained for all the masks tested, as well as the free cough in order to compare them. Clear differences are detected between not using any kind of protective equipment, not only in maximum penetration values, but in the slope of the penetration curves, which has already been seen by performing the curve fitting previously. The cloth mask curves can also be differentiated from the other two masks, as it also reaches spray tip travel distance higher than 100 mm, while the Surgical and FFP2 masks superimpose their curves when compared, although the slopes of the FFP2 curves have been observed to be slightly lower than the surgical mask ones.

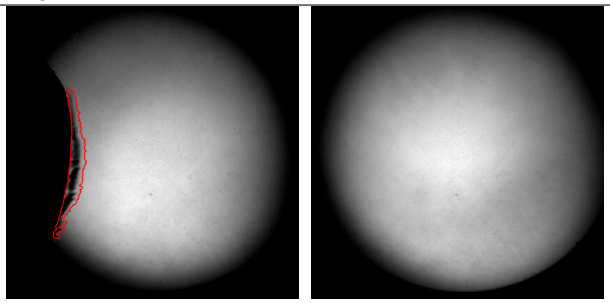

(a) t = 40 ms - Window 1 (b) t = 40 ms - Window 2

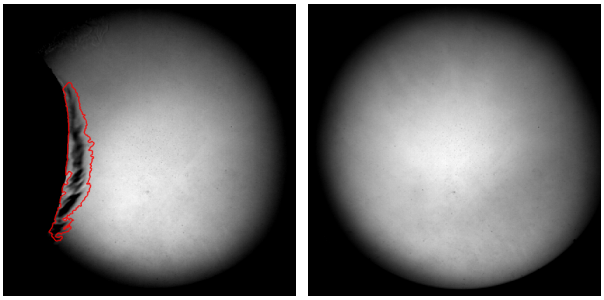

(c) t = 80 ms - Window 1 (d) t = 80 ms - Window 2

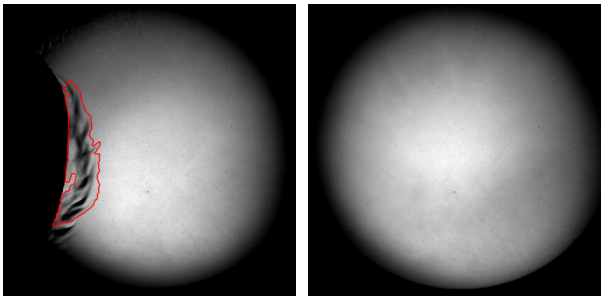

(e) t = 120 ms - Window 1 (f) t = 120 ms - Window 2

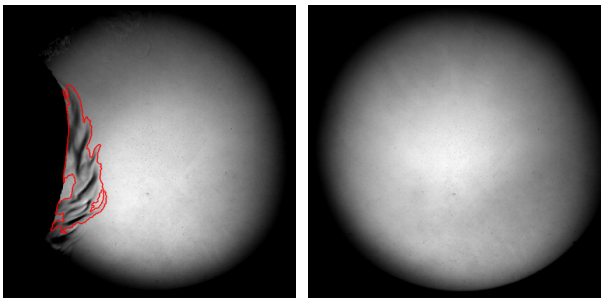

(g) t = 160 ms - Window 1 (h) t = 160 ms - Window 2

Figure 14: Time snapshots of the cough contour for the strongest flow rate profile time profile and the surgical mask at the two positions of the Schlieren experiment.

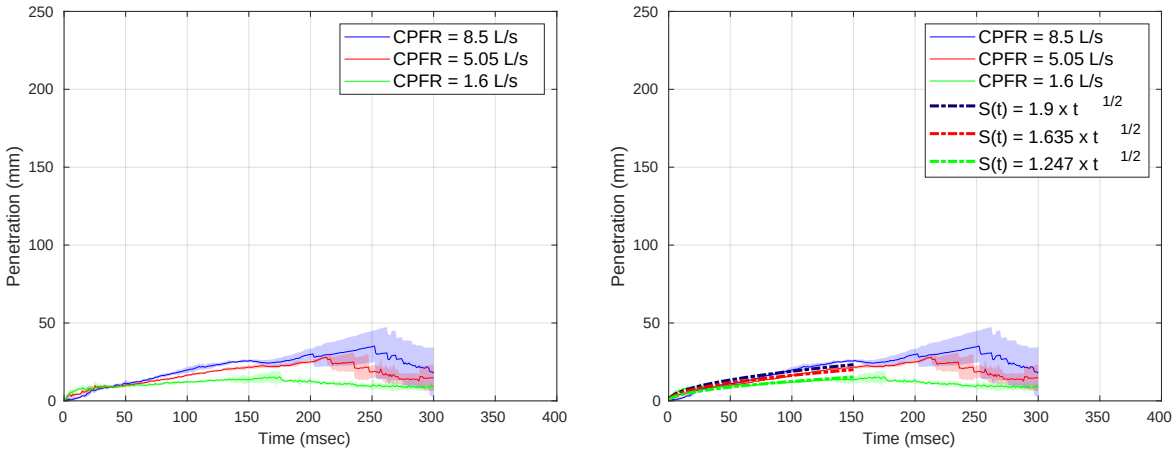

(a) Distance curves

(b) Curve fitting

Figure 15: Distances with respect to the surgical mask, at the three CPFR time profiles and its corresponding curve regression.

4. Conclusions

Due to the recent need to increase the knowledge regarding transmission ways of airborne pathogens, an experimental facility has been built around a mannequin head to obtain the main human cough characteristics, as well as to assess the effectiveness of the different face masks that are available to the public to prevent contagion. From them, the following conclusions have been extracted:

- Employing a mannequin head that includes realistic aerial cavities allows to reduce uncertainties of analysing the human cough, and increases the repeatability, as literature reports high variability in the results by employing real participants.
- The Schlieren imaging technique used shows penetration distances of 400 mm for all the tested CPFR profiles, being this the maximum value that could be detected by the employed test rig. Further penetration values should be expected for all of the tested conditions. As literature reports that droplet trajectories are directly controlled by air flow dynamics, this method also allows to assess the pathogen dispersion.
- As the CO_2 is expelled while exhaling, substituting air by this gas in order to enhance density gradients is a feasible approach, as the penetration curves show the same dependency with time ($S \propto t^{\frac{1}{2}}$) during the jet phase as previous literature studies.
- From the data collected from fitting face masks to the mannequin head, the penetration values are significantly reduced for the surgical and FFP2 masks. On the other hand, cloth masks, although it diminishes the velocity of the exhaled gases, it only reduces it by a 50%. Surgical mask showed a maximum travelled distance of 30 mm, and 21 mm for the FFP2 respirator. In consequence, the cloth mask is not recommended to stop human coughs and therefore to prevent virus transmission.
- FFP2 showed the best results in terms of cough propagation, preventing it completely for weak coughs. Nonetheless, according to the density gradient visualization, it is important to properly fit the respirator around the mouth and nose, as some leakages were detected. Surgical masks, in the other hand did not show such leakages, but showed slightly greater penetration lengths.

  Coughing without any protective equipment has been shown to be a feasible virus transmitter. Future studies could take advantage of the employed cough replication methodology and generate droplets to assess also the filtering capabilities of such masks. Coughing in turbulent environment such as the ones induced by air

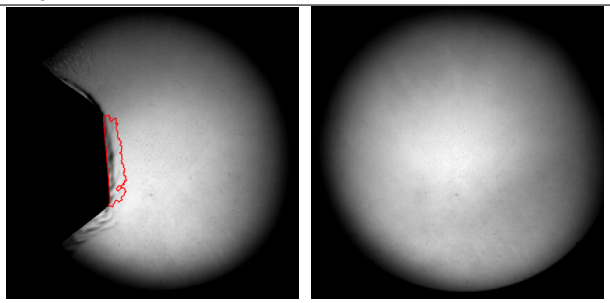

(a) t = 40 ms - Window 1 (b) t = 40 ms - Window 2

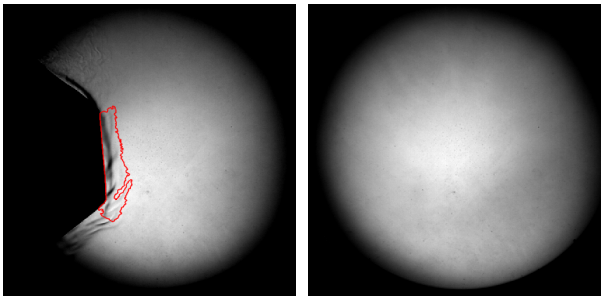

(c) t = 80 ms - Window 1 (d) t = 80 ms - Window 2

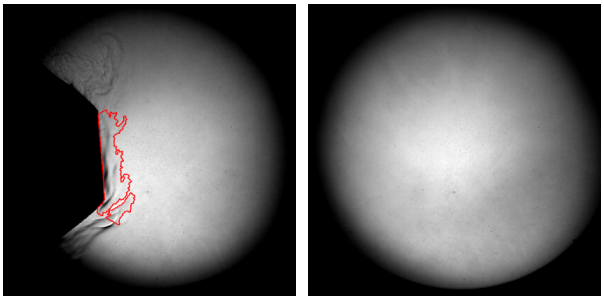

(e) t = 120 ms - Window 1 (f) t = 120 ms - Window 2

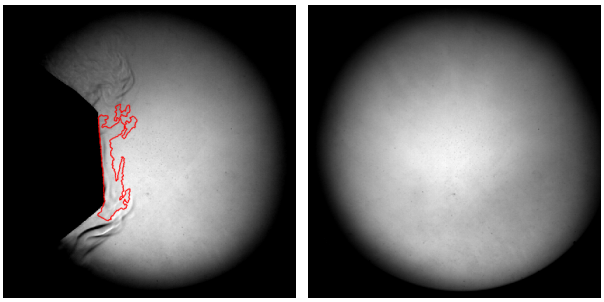

(g) t = 160 ms - Window 1 (h) t = 160 ms - Window 2

Figure 16: Time snapshots of the cough contour for the strongest flow rate profile time profile and the FFP2 respirator at the two positions of the Schlieren experiment.

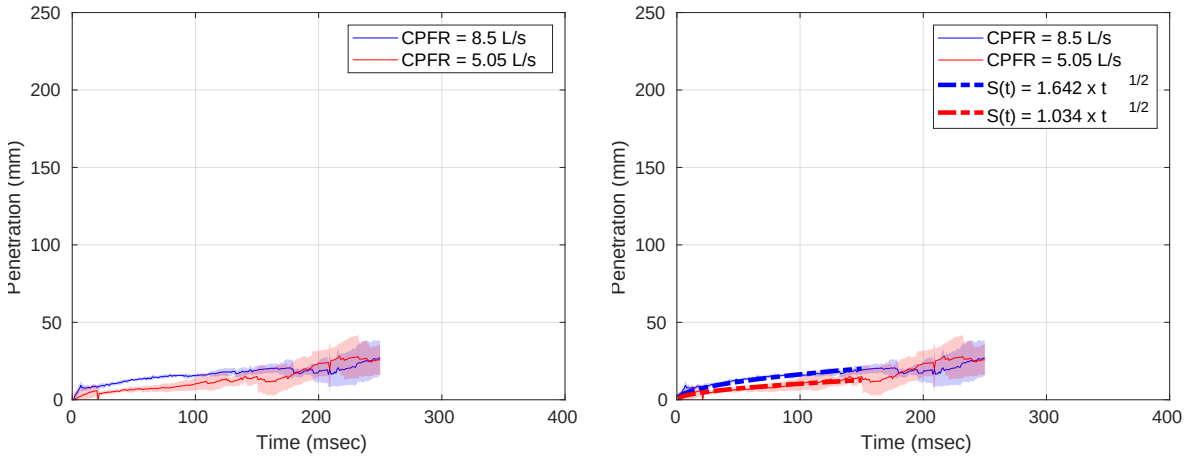

(a) Distance curves

(b) Curve fitting

Figure 17: Distances with respect to the FFP2 respirator, at the three CPFR time profiles and its corresponding curve regression.

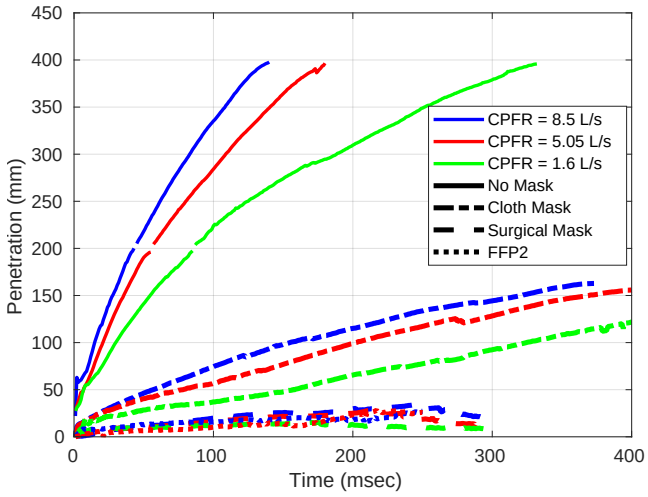

Figure 18: Penetration curves for all the test conditions performed.

conditioning systems could alter the parameters studied, and consequently modify the transmission ways of airborne viruses. This could modify prevention techniques in those situations and therefore its study is highly encouraged. In addition to it, further studies should consider the effect of the cough temperature, as the lower density and hence the changes in viscosity should vary up to a certain degree the macroscopic characteristics of the cough jet. Moreover, proportional valves could substitute the on/off valves employed in order to achieve a higher degree of similarity between the experimental and literature curves.

References

[1] L. Morawska, Droplet fate in indoor environments, or can we prevent the spread of infection?, Indoor Air 16 (5) (2006) 335–347. doi:10.1111/j.1600-0668.2006.00432.x.

[2] J. P. Duguid, The size and the duration of air-carriage of respiratory droplets and droplet-nuclei, Journal of Hygiene 44 (6) (1946) 471–479. doi:10.1017/S0022172400019288.

[3] W. G. Lindsley, J. S. Reynolds, J. V. Szalajda, J. D. Noti, D. H. Beezhold, A Cough Aerosol Simulator for the Study of Disease Transmission by Human Cough-Generated Aerosols., Aerosol science and technology : the journal of the American Association for Aerosol Research 47 (8) (2013) 937–944. doi:10.1080/02786826.2013.803019.

[4] C. Y. Chao, M. P. Wan, L. Morawska, G. R. Johnson, Z. D. Ristovski, M. Hargreaves, K. Mengersen, S. Corbett, Y. Li, X. Xie, D. Katoshevski, Characterization of expiration air jets and droplet size distributions immediately at the mouth opening, Journal of Aerosol Science 40 (2) (2009) 122–133. doi:10.1016/j.jaerosci.2008.10.003.

[5] R. G. Loudon, R. M. Roberts, Droplet expulsion from the respiratory tract., American Review of Respiratory Disease 95 (3) (1967) 435–442. doi:10.1164/arrd.1967.95.3.435.

[6] X. Xie, Y. Li, H. Sun, L. Liu, Exhaled droplets due to talking and coughing, Journal of The Royal Society Interface 6 (dec 2009). doi:10.1098/rsif.2009.0388.focus.

[7] G. Zayas, M. C. Chiang, E. Wong, F. MacDonald, C. F. Lange, A. Senthilselvan, M. King, Cough aerosol in healthy participants: Fundamental knowledge to optimize droplet-spread infectious respiratory disease management, BMC Pulmonary Medicine 12 (March) (2012). doi:10.1186/1471-2466-12-11.

[8] G. R. Johnson, L. Morawska, Z. D. Ristovski, M. Hargreaves, K. Mengersen, C. Y. Chao, M. P. Wan, Y. Li, X. Xie, D. Katoshevski, S. Corbett, Modality of human expired aerosol size distributions, Journal of Aerosol Science 42 (12) (2011) 839–851. doi:10.1016/j.jaerosci.2011.07.009.

[9] H. Wang, Z. Li, X. Zhang, L. Zhu, Y. Liu, S. Wang, The motion of respiratory droplets produced by coughing, Physics of Fluids 32 (12) (2020). arXiv:2010.12781, doi:10.1063/5.0033849.

[10] Z. T. Ai, A. K. Melikov, Airborne spread of expiratory droplet nuclei between the occupants of indoor environments: A review., Indoor air 28 (4) (2018) 500–524. doi:10.1111/ina.12465.

[11] N. Sen, Transmission and evaporation of cough droplets in an elevator: Numerical simulations of some possible scenarios, Physics of Fluids 33 (3) (2021) 33311. doi:10.1063/5.0039559.

[12] L. Borro, L. Mazzei, M. Raponi, P. Piscitelli, A. Miani, A. Secinaro, The role of air conditioning in the diffusion of Sars-CoV-2 in indoor environments: A first computational fluid dynamic model, based on investigations performed at the Vatican State Children's hospital, Environmental Research 193 (2021) 110343. doi:https://doi.org/10.1016/j.envres.2020.110343.

[13] V. Vuorinen, M. Aarnio, M. Alava, V. Alopaeus, N. Atanasova, M. Auvinen, N. Balasubramanian, H. Bordbar, P. Erästö, R. Grande, N. Hayward, A. Hellsten, S. Hostikka, J. Hokkanen, O. Kaario, A. Karvinen, I. Kivistö, M. Korhonen, R. Kosonen, J. Kuusela, S. Lestinen, E. Laurila, H. J. Nieminen, P. Peltonen, J. Pokki, A. Puisto, P. Råback, H. Salmenjoki, T. Sironen, M. Österberg, Modelling aerosol transport and virus exposure with numerical simulations in relation to SARS-CoV-2 transmission by inhalation indoors, Safety Science 130 (2020) 104866. doi:10.1016/j.ssci.2020.104866.

[14] J. K. Gupta, C.-H. Lin, Q. Chen, Flow dynamics and characterization of a cough, Indoor Air 19 (6) (2009) 517–525. doi:10.1111/j.1600-0668.2009.00619.x.

[15] S. Ren, J. Niu, M. Cai, L. Hao, Y. Shi, W. Xu, Z. Luo, Novel assisted cough system based on simulating cough airflow dynamics, Bio-Design and Manufacturing 4 (3) (2021) 479–489. doi:10.1007/s42242-021-00132-9.

[16] J. Wei, Y. Li, Enhanced spread of expiratory droplets by turbulence in a cough jet, Building and Environment 93 (P2) (2015) 86–96. doi:10.1016/j.buildenv.2015.06.018.

[17] P. M. de Oliveira, L. C. Mesquita, S. Gkantonas, A. Giusti, E. Mastorakos, Evolution of spray and aerosol from respiratory releases: Theoretical estimates for insight on viral transmission, medRxiv (2020). doi:10.1101/2020.07.23.20160648.

[18] J. Muthusamy, S. Haq, S. Akhtar, M. A. Alzoubi, T. Shamim, J. Alvarado, Implication of coughing dynamics on safe social distancing in an indoor environment—A numerical perspective, Building and Environment 206 (2021) 108280. doi:10.1016/j.buildenv.2021.108280.

[19] H. Li, F. Y. Leong, G. Xu, C. W. Kang, K. H. Lim, B. H. Tan, C. M. Loo, Airborne dispersion of droplets during coughing: a physical model of viral transmission, Scientific Reports 11 (1) (2021) 4617. doi:10.1038/s41598-021-84245-2.

[20] S. Verma, M. Dhanak, J. Frankenfield, Visualizing the effectiveness of face masks in obstructing respiratory jets, Physics of Fluids 32 (6) (2020). doi:10.1063/5.0016018.

[21] L. Bourouiba, E. Dehandschoewercker, J. W. Bush, Violent expiratory events: On coughing and sneezing, Journal of Fluid Mechanics 745 (2014) 537–563. doi:10.1017/jfm.2014.88.

[22] P. H. Geoghegan, A. M. Laffra, N. K. Hoogendorp, M. C. Taylor, M. C. Jermy, Experimental measurement of breath exit velocity and expirated bloodstain patterns produced under different exhalation mechanisms, International Journal of Legal Medicine 131 (5) (2017) 1193–1201. doi:10.1007/s00414-017-1545-2.

[23] M. VanSciver, S. Miller, J. Hertzberg, Particle Image Velocimetry of Human Cough, Aerosol Science and Technology 45 (3) (2011) 415–422. doi:10.1080/02786826.2010.542785.

[24] N. Dudalski, A. Mohamed, S. Mubareka, R. Bi, C. Zhang, E. Savory, Experimental investigation of far-field human cough airflows from healthy and influenza-infected subjects, Indoor Air 0 (2020) 1–12. doi:10.1111/ina.12680.

[25] P. Prasanna Simha, P. S. Mohan Rao, Universal trends in human cough airflows at large distances, Physics of Fluids 32 (8) (2020). doi:10.1063/5.0021666.

[26] P. Forouzandeh, K. O'Dowd, S. C. Pillai, Face masks and respirators in the fight against the COVID-19 pandemic: An overview of the standards and testing methods, Safety Science 133 (2021) 104995. doi:10.1016/j.ssci.2020.104995.

[27] G. Tanisali, A. Sozak, A. S. Bulut, T. Z. Sander, O. Dogan, Ç. Dağ, M. Gönen, F. Can, H. DeMirci, O. Ergonul, Effectiveness of different types of mask in aerosol dispersion in SARS-CoV-2 infection, International Journal of Infectious Diseases 109 (2021) 310–314. doi:10.1016/j.ijid.2021.06.029.

[28] G. S. Settles, Schlieren and Shadowgraph Techniques, Springer Berlin Heidelberg, 2001.

[29] R. Dhand, J. Li, Coughs and Sneezes: Their Role in Transmission of Respiratory Viral Infections, Including SARS-CoV-2, American journal of respiratory and critical care medicine 202 (5) (2020) 651–659. doi:10.1164/rccm.202004-1263PP.

[30] N. M. Tsoukias, Z. Tannous, A. F. Wilson, S. C. George, Single-exhalation profiles of NO and CO2 in humans: effect of dynamically changing flow rate., Journal of applied physiology (Bethesda, Md. : 1985) 85 (2) (1998) 642–652. doi:10.1152/jappl.1998.85.2.642.

[31] P. Höppe, Temperatures of expired air under varying climatic conditions, International Journal of Biometeorology 25 (2) (1981) 127–132. doi:10.1007/BF02184460.

[32] J. Korpas, M. Vrabec, J. Sadlonova, D. Salat, L. A. Debreczeni, Analysis of the cough sound frequency in adults and children with bronchial asthma., Acta physiologica Hungarica 90 (1) (2003) 27–34. doi:10.1556/APhysiol.90.2003.1.4.

[33] A. K. Lichtarowicz, R. K. Duggins, E. Markland, Discharge coefficients for incompressible non-cavitating flow through long orifices, Journal of Mechanical Engineering Science 7 (2) (1965) 210–219. doi:10.1243/JMES_JOUR_1965_007_029_02.

[34] S. Rengasamy, D. Sbarra, J. Nwoko, R. Shaffer, Resistance to synthetic blood penetration of National Institute for Occupational Safety and Health-approved N95 filtering facepiece respirators and surgical N95 respirators, American Journal of Infection Control 43 (11) (2015) 1190–1196. doi:https://doi.org/10.1016/j.ajic.2015.06.014.

[35] M. Khosravi, G. McTaggart-Cowan, P. Kirchen, Pyrometric imaging of soot processes in a pilot ignited direct injected natural gas engine, International Journal of Engine Research 22 (5) (2020) 1605–1623. doi:10.1177/1468087420919196.

[36] R. Payri, F. J. Salvador, R. Abboud, A. Viera, Study of evaporative diesel spray interaction in multiple injections using optical diagnostics, Applied Thermal Engineering 176 (May) (2020) 115402. doi:10.1016/j.applthermaleng.2020.115402.

[37] R. Payri, F. J. Salvador, G. Bracho, A. Viera, Differences between single and double-pass schlieren imaging on diesel vapor spray characteristics, Applied Thermal Engineering 125 (2017) 220–231. doi:10.1016/j.applthermaleng.2017.06.140.

[38] R. Payri, J. P. Viera, V. Gopalakrishnan, P. G. Szymkowicz, The effect of nozzle geometry over internal flow and spray formation for three different fuels, Fuel 183 (2016) 20–33. doi:https://doi.org/10.1016/j.fuel.2016.06.041.

[39] EN, Medical face masks – Requirements and test methods- EN14683:2019+AC:2019 (2019).

[40] R. Sommerstein, C. A. Fux, D. Vuichard-Gysin, M. Abbas, J. Marschall, C. Balmelli, N. Troillet, S. Harbarth, M. Schlegel, A. Widmer, C. Balmelli, M.-C. Eisenring, S. Harbarth, J. Marschall, D. Pittet, H. Sax, M. Schlegel, A. Schweiger, L. Senn, N. Troillet, A. F. Widmer, G. Zanetti, Swissnoso, Risk of SARS-CoV-2 transmission by aerosols, the rational use of masks, and protection of healthcare workers from COVID-19, Antimicrobial Resistance & Infection Control 9 (1) (2020) 100. doi:10.1186/s13756-020-00763-0.

[41] European Committee for Standardization, Respiratory protective devices - Filtering half masks to protect against particles - Requirements, testing, marking (2009).

[42] R. Mittal, R. Ni, J.-H. Seo, The flow physics of COVID-19, Journal of Fluid Mechanics 894 (2020) F2. doi:DOI:10.1017/jfm.2020.330.

[43] A. H. Lefebvre, V. G. McDonell, Atomization and sprays, 2nd Edition, Press, CRC, Boca Raton, FL, 2017. doi:10.1201/9781315120911.

[44] R. Payri, P. Martí-Aldaraví, P. M. Quintero, J. Marco-Gimeno, Large eddy simulation for the prediction of human coughing (2021). doi:10.1615/ATOMIZSPR.2021037129.

[45] S. A. Chillón, A. Ugarte-Anero, I. Aramendia, U. Fernandez-Gamiz, E. Zulueta, Numerical Modeling of the Spread of Cough Saliva Droplets in a Calm Confined Space (2021). doi:10.3390/math9050574.

[46] J. W. Tang, T. J. Liebner, B. A. Craven, G. S. Settles, A schlieren optical study of the human cough with and without wearing masks for aerosol infection control, Journal of the Royal Society Interface 6 (2009) 727–736. doi:10.1098/rsif.2009.0295.focus.